Long-range time-of-flight scanning sensor based on high-speed time-correlated single-photon counting

Aongus McCarthy,[1] Robert J. Collins,[1] Nils J. Krichel,[1] Verónica Fernández,[1,2] Andrew M. Wallace,[1] and Gerald S. Buller[1,*]

[1]School of Engineering and Physical Sciences, Heriot-Watt University, Riccarton, Edinburgh, UK, EH14 4AS

[2]Now at Instituto de Física Aplicada, Consejo Superior de Investigaciones Científicas, Serrano 144, 28006 Madrid, Spain

*Corresponding author: G.S.Buller@hw.ac.uk

Received 7 July 2009; revised 11 October 2009; accepted 12 October 2009; posted 13 October 2009 (Doc. ID 113822); published 4 November 2009

We describe a scanning time-of-flight system which uses the time-correlated single-photon counting technique to produce three-dimensional depth images of distant, noncooperative surfaces when these targets are illuminated by a kHz to MHz repetition rate pulsed laser source. The data for the scene are acquired using a scanning optical system and an individual single-photon detector. Depth images have been successfully acquired with centimeter *xyz* resolution, in daylight conditions, for low-signature targets in field trials at distances of up to 325 m using an output illumination with an average optical power of less than 50 μW. © 2009 Optical Society of America

OCIS codes: 280.3400, 120.3930, 040.3780, 150.6910.

1. Introduction

In recent years, application areas for three-dimensional imaging have emerged in several fields, including manufacturing [1], defense [2], and geosciences [3]. Several groups have acquired depth information and constructed depth images using variations of the time-correlated single-photon counting technique (TCSPC) [4–9]. The TCSPC approach to laser radar affords a number of potential advantages over non-photon-counting approaches. These potential advantages include improved depth resolution [10] over linear multiplication detector-based systems [11]. The improved depth resolution means that TCSPC can be effectively utilized in the identification of distributed targets where the scattering surfaces are closely separated [12]. The advantage of shot-noise-limited detection of single-photon events means that the system can be used even when there is an average of less than one photon return event per pulse, which is critical in applications involving long-distance ranging [5]. At kilometer ranges, the low photon return rates permit the use of high repetition rate, compact, low-power laser diodes, since it is not necessary to record a return on every outgoing laser pulse. The TCSPC technique does have several potential disadvantages, including the following: limited spectral range of practical single-photon detectors [13]; detector dead time where the detection system is shut down to reset after the recording of an event [14]; and issues regarding solar background events providing potential false alarms [15]. Nonetheless, there is growing interest in depth imaging using TCPSC, especially as photon-counting detector and acquisition technology continues to improve, permitting faster data acquisition at longer range.

The general approach of photon-counting ranging has been to direct a pulsed laser toward a noncooperative target (i.e., an object or scene that does not lend itself to reflecting the transmitted laser pulses back toward the source) with the scattered photon return being recorded by a photon-counting detector. Timing information from the recorded photon returns is used to determine the round-trip time, which subsequently is employed to calculate the distance to

0003-6935/09/326241-11$15.00/0

the target. Each transmitted pulse and photon return constitutes an individual measurement of the distance to the target. Statistical analysis of many of these independent measurements (typically 10^3–10^6) can yield a time-of-flight resolution that is better than the overall timing jitter of the system. In prior work [8,16,17], we constructed a system based on TCSPC for performing depth image measurements in indoor environments under typically low ambient light level conditions at standoff distances of around 10 m. This used a large pan-and-tilt head mechanism to scan a compact optical system containing an optimized silicon single-photon avalanche diode (SPAD) detector. In parallel, we developed a kilometer range system, based on a commercially available 200 mm diameter aperture Schmidt–Cassegrain telescope for single point use in target identification under daylight conditions [12].

Time-of-flight imaging systems using *arrays* of single-photon detectors have been reported, for example, by Priedhorsky *et al.* [9], who proposed a system using a microchannel plate with cross-channel delay line to provide time-of-flight information with $x-y$ spatial information. This proposal was demonstrated later by Ho *et al.* [6] in both indoor and outdoor environments over a range of 50 m. More recently, a group at the Massachusetts Institute of Technology Lincoln Labs demonstrated photon-counting time-of-flight using 4×4 arrays of detectors [4] and scanning mirrors with measurements at ranges of 60 m shown for target objects in daylight. Later, the group made time-of-flight measurements using a 32×32 photon-counting detector array [7] and a rotating Risley prism beam steering arrangement to form depth images at ranges of 150 m. In [5], Degnan describes a low dead-time photon-counting system used as a time-of-flight microaltimeter capable of measuring multiple return events from a single laser pulse, using a microchannel plate photomultiplier approach. In this case, the source was operating at kHz repetition rates and the system exhibited measurements at altitudes of several km.

While arrayed detectors can provide advantages in terms of parallelism, there can be issues with cross talk and fill factor [18], in particular. Here we present a scanning time-of-flight depth sensor that uses a commercially available individual, ungated single-photon counting detector module. The high-performance single-photon detector module is fiber-coupled to a compact optical transceiver head that contains a pulsed laser diode and a pair of galvanometer scanning mirrors. These mirrors are used to scan both the outgoing laser beam and the collected return photons—meaning that a single optimized detector can be used to obtain a complete three-dimensional image. The single-mode optical fiber delivery method means the system can be easily reconfigured for use with alternative single-photon detector technologies and the fiber also acts as a convenient and effective spatial filter for background light. Unlike many of the other systems described, this system is configured for low energy optical pulses (typically <30 pJ or fewer than $\sim 130 \times 10^6$ photons per pulse) and this means that multiple photon returns from a single output pulse are improbable. This low probability helps to minimize the number of collected return photons that go undetected—a single triggering detector is used and, once a photon event has been recorded, the subsequent detector dead time (currently ~ 100 ns) means that it is unable to register any additional photons arriving in this period. We utilize low energy optical pulses ($\sim$pJ) for this work in conjunction with a potentially high repetition rate laser source (tens of MHz) to reduce the data acquisition time. The inherent time gating and high sensitivity of the TCSPC approach and effective spatial and spectral filtering permit daytime and nighttime operation at eye-safe laser power levels. The system has been used in daylight conditions to construct depth images with centimeter spatial and depth resolution of noncooperative targets at a range of 325 m using μW average output power levels. This range distance does not represent a limitation of the system, but instead was dictated by available target range facilities during these field trials. The two scanning mirrors are common to both the transmit and the receive channels and enable the scene to be scanned much faster compared with the relatively slow data acquisition process when using the pan-and-tilt head of our previous system [17]. The coaxial optical arrangement means that the transmitted beam is directed selectively, only at the field point being ranged, leading to the most efficient use of the low-power source. In the measurements shown below, the average power of the output illumination used was less than 50 μW.

The system described here is shown schematically in Fig. 1 and a summary of the main system parameters is listed in Table 1. The system uses a picosecond-pulsed semiconductor diode laser whose output is scanned across the scene of interest by a galvanometer mirror pair. The laser typically operates at kHz to MHz repetition rates, with the average transmitted optical power being between 1 μW and 1 mW. The scattered optical return from the distant target is collected by the same optical system from

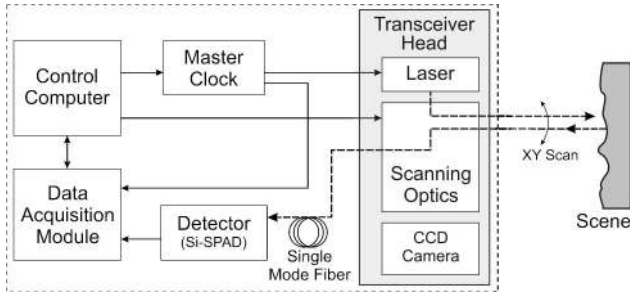

Fig. 1. Schematic diagram indicating the principal components of the scanning system. The scene typically is at a range of hundreds of meters to several km. Electrical paths are denoted by solid lines and optical paths by dashed lines. Si-SPAD is a silicon single-photon avalanche diode.

Table 1. Summary of the Scanning Sensor System Parameters

Parameter	Value / Comment
Transmit/receive alignment	Mono-static, i.e., transmit and receive channels are coaxial
Laser wavelength λ	~842 nm
Laser type	Pulsed semiconductor diode
Laser pulse width	~90 ps, full width at half-maximum
Optical output power P_{Out}	$<50\,\mu$W average
Detector	Si-SPAD, Single-Photon Counting Module (Perkin Elmer), Active area diameter 180 μm, thick junction, ~400 ps jitter, fiber-coupled (~5 μm diameter core, armored fiber)
Beam scanning mechanism	Galvanometer mirror pair ($x-y$) (common to both the transmit and receive channels)
System objective	200 mm focal length, $f/2.8$ (Canon EF camera lens)
Receive aperture diameter	72 mm
System $f/\#$	$f/4$
Field of view	Total available for scanning: ~55 mrad (17 m diameter at 325 m) Single point: ~70 μrad (22 mm diameter at 325 m). The control software allows the user to set the xy extent of the scan within the available field of view, and the number of "pixels" in x and y.
Range	Scans carried out at, but not limited to, ranges from 5 to 330 m.
System resolution at 325 m	Spatial (xy): ~20 mm Depth (range): As low as 20 mm. The depth resolution is dependent on a number of factors but primarily the number of detected return photons (the longer the acquisition time the better the resolution).

which the laser pulse is emitted and redirected using polarization optics to a single-mode optical fiber detection channel. This fiber is connected to a single-photon detector module and the output signal from the detector is recorded as time-tagged photon events that are continuously streamed to the control computer. The control software reconciles this timing information with field position to calculate depths at individual target positions and, thus, produce a depth image across the scanned field.

2. Optical Design and Optomechanics

A schematic diagram of the optical system is shown in Fig. 2. An interchangeable commercially available single lens reflex (SLR) camera lens is used as the system objective. This objective is used to direct the outgoing laser to the target and also to efficiently collect the scattered photons returned from the target. For the experiments detailed in this paper, the objective was a 200 mm effective focal length,

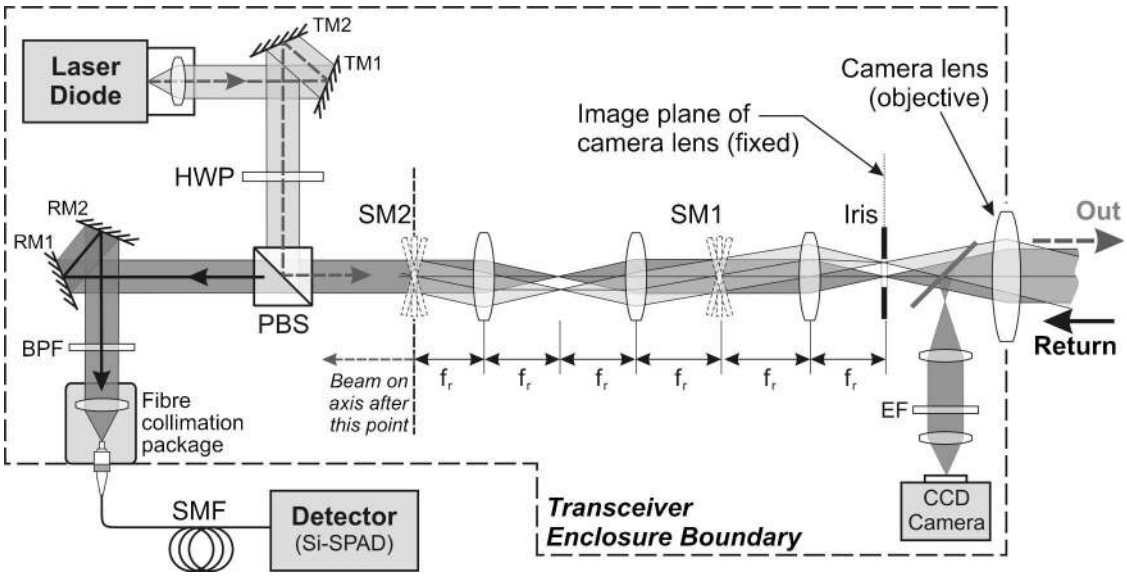

Fig. 2. Schematic of the optical layout. The pulsed output of the laser diode is incident on a pair of steering mirrors (TM1, TM2), passes through a half-wave plate (HWP), a polarizing beam splitter (PBS), two galvanometer scanning mirrors (SM1, SM2), relay optics and exits the transceiver head through the camera lens objective. A small percentage of the incoming light is reflected into a monitoring channel where an edge filter (EF) is used to block the laser transmission. The return path goes through the same scanning and relay optics as the laser beam, passes through the beam splitter, onto a pair of steering mirrors (RM1, RM2) and is spectrally filtered by a bandpass filter (BPF) before being coupled into an ~5 μm core diameter single-mode fiber (SMF) by a fiber collimation package. The fiber is connected to the single photon avalanche diode (SPAD) detector module.

nine-element Canon camera lens with an f number of $f/2.8$.

The required part of the scene is relayed to the optical fiber core (which is connected to the single-photon detector) via the imaging optics and a pair of computer-controlled galvanometer scanning mirrors. The mirrors SM1 and SM2 as shown in Fig. 2 and the required lenses are arranged in a spatially separated telecentric relay configuration. The scanning mirrors are placed at conjugate planes of the system and, as a result, the point at which the transmit and receive beams are incident on the mirrors remains stationary as they are scanned. Three identical five-element, 30 mm focal length lenses [19], operating at infinite conjugates are used for the relay optics. This five-element lens design has a flat field, diffraction-limited performance at 850 nm and is corrected for $f \sin\Theta$ distortion. An 11 mm focal length fiber collimation package is used to couple the light into a small ($<10\,\mu$m) diameter optical fiber core connected to the detector. This arrangement provides an effective means of spatially filtering the background illumination, such as solar background and off-axis light.

The maximum field of view that can be scanned by this sensor is primarily set by the field of view of the image presented to the internal system optics by the objective lens, and the field of view of the 30 mm focal length relay lenses, the latter being the limiting factor. The 200 mm focal length objective and 30 mm focal length relay lens combination used for the work described in this paper has a maximum full field of view of 55 mrad. The spatial resolution achieved depends on a number of factors including the focal lengths of the lenses, the aberrations of the optics, and, in particular, the size of the fiber core coupled to the detector. When the system was aligned and focused on the scene at 325 m, the aperture of the receive channel when using a $5\,\mu$m diameter core fiber was measured to be approximately 25 mm in diameter with the transmit channel laser beam diameter being slightly larger. This beam diameter equates to a spatial resolution of approximately 70 mm at a 1 km range and corresponds to the minimum angular step resolution of the galvanometer mirrors used in the measurements shown below.

The sensor head consists of a custom-built optomechanical assembly that uses a slotted-baseplate approach for mounting the majority of the optical components [20]. A 25 mm thick plate of aluminum, with an appropriate network of slots of a fixed width machined into its surface, is used as the baseplate for this sensor. The optical components and devices are mounted in 35 mm diameter magnetic steel barrels, which in turn are placed in the baseplate slots and held in position with magnets. The combination of slot width and barrel diameter defines an optic axis which, in this case, is 14 mm above the top surface of the baseplate. This optomechanical system provides a convenient and robust semi-kinematic mount that combines good long-term mechanical stability under typical laboratory conditions, with the possibility of reconfiguration and ease of alignment. The objective lens is attached to the baseplate using a Canon lens fitting adaptor plate—thus enabling any lens with a compatible fitting to be used with the system. The aluminum baseplate, sidewalls and lid that make up the enclosure were surface finished with an $\sim 10\,\mu$m thick black anodized coating to protect the aluminum while handling as well as helping to minimize internal stray light levels. The completed sensor head is shown in Fig. 3 and measures $\sim 275\,\text{mm} \times 275\,\text{mm} \times 170\,\text{mm}$.

The transmit and receive channels of the system were aligned to be coaxial so that the image of the receiver collection fiber core was concentric with the transmitted laser beam, irrespective of the range. This was achieved by monitoring the near-field and far-field alignment of the transmit and receive channels while adjustments were made using a pair

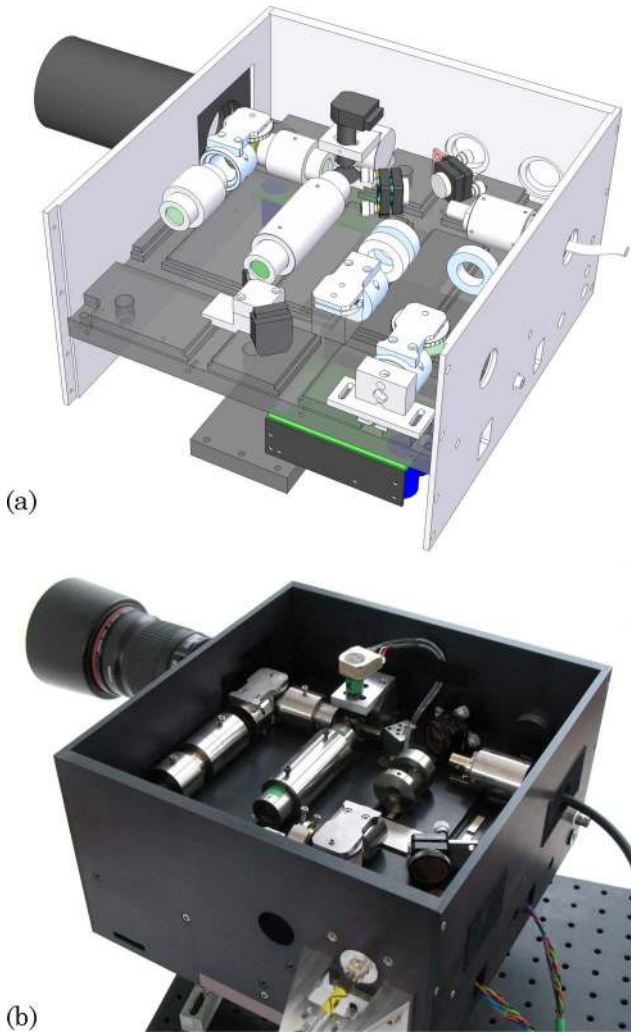

Fig. 3. (Color online) Transceiver head assembly: (a) Three-dimensional image produced from the CAD model of the system showing the enclosure ($\sim 275 \times 275 \times 170$ mm) and the slotted-baseplate optomechanics. The two galvanometer servo-control circuit boards are housed on the underside of the slotted baseplate. (b) Photograph of the assembled transceiver head.

of adjustable steering mirrors in both of the channels. The sensor head maintained its optical alignment over several months of operation in the field laboratory environment where the temperature varied between approximately 10 °C and 25 °C.

3. Control Electronics and Data Acquisition

The master clock for the system used when acquiring the results shown in this paper was a commercially available pulse pattern generator, which served to synchronize and gate the TCSPC electronics and clock the laser pulses over a frequency range of a few kHz to 2 MHz. The laser was an ~90 picosecond pulse-width laser diode operating at a central wavelength of ~842 nm and the output power was controlled by a variable current driving unit.

The output laser pulses and returned photons were scanned using a pair of galvanometer mirrors, one providing adjustment of the vertical (y) position and one providing adjustment of the horizontal (x) position. Each of the mirrors was driven by a servo-control circuit board and the position command input signals for these boards was set by the system control software through a computer-based digital-to-analog converter card.

Data acquisition was performed using a PicoHarp 300 TCSPC module, manufactured by PicoQuant GmbH. Photons returned from the target and successfully collected by the objective lens were measured using a fiber-coupled silicon single-photon avalanche diode (Si-SPAD). In this case a free-running commercially available (Perkin Elmer) thick junction silicon detector with an active area diameter of 180 μm was used, although other fiber-coupled single-photon detectors can be connected for future measurements. The optical head was connected to the Si-SPAD using an ~5 μm diameter core optical fiber with an angle polished connector (APC) to minimize optical backreflections, which would appear as ghost secondary peaks in the target return histogram (see Section 4).

4. Software

A. Hardware Control

The system was controlled by a desktop personal computer (PC) running custom software developed in house. The current iteration of the software was designed for maximum flexibility in testing and development and was not optimized for speed of operation or processing. The TCSPC module was operated in time-tagged mode so that the times of events on each of the two inputs were recorded independently, but relative to a common macrotime. One input was the synchronization signal from the master clock indicating the time at which a laser pulse was emitted, the other was the signal from the Si-SPAD, indicating the time of a photon return.

The camera lens that is used as the system objective introduced a backreflection into the return photon path, which resulted in a system return peak in the histogram containing a high number of integrated counts. The TCSPC electronics had a maximum count rate of approximately four million events per second across both input channels. Photons detected from the backreflection cause a high percentage of the overall photon return rate and do not contribute to depth profile measurements. The TCSPC electronics have an input that suspends acquisition of photon events when the transistor–transistor logic (TTL) voltage applied to it is in a low logic level. A signal from the master clock was used to suspend registration of photon events during the expected period of the internal optical backreflection, as shown in Fig. 4. This reduced the overall recorded count per second rate at the TCSPC electronics and permitted the use of higher laser pulse repetition frequencies. The relative time and duration of the electrical gate could be adjusted as required by the experimental conditions.

B. Data Acquisition and Analysis

To acquire a depth profile, the galvanometer mirrors steer the laser beam in a raster pattern over the specified field of view in a move–stop–move motion. The control software allows the user to set the xy extent of the scan within the available field of view, the number of pixels in x and y, and the pixel dwell time. The TCSPC electronics commences the acquisition of photon return events at the beginning of a frame and continuously streams photon return data until the end of the frame. To mark the beginning of the frame and the end of each line, a low resolution (~10 ns FWHM timing jitter) marker is inserted into the raw time stream data. The analysis software subdivides the collected time stream data at each of these markers to produce a fixed number of lines, and then further subdivides each line into the appropriate number of individual pixels.

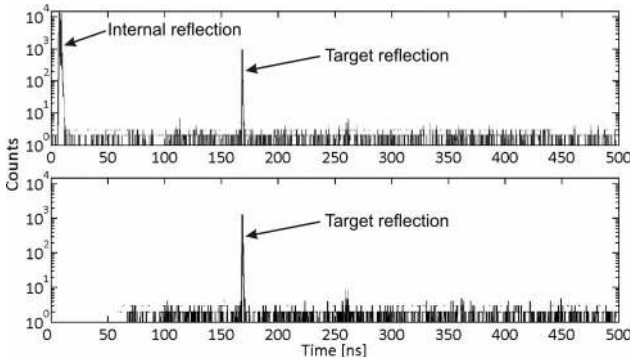

Fig. 4. Example histograms taken on a retroreflective reference material. Both measurements were taken with a 1 s acquisition time and feature comparable target return peaks around 165 ns. The high repetition rate of the system results in multiple photon pulses being in transit at any given point and causes distant target returns to be assigned to short flight times. The lower plot demonstrates the hardware gating functionality: reducing the duty cycle to 80% removed significant photon returns caused by internal optical reflections of the system.

The two independent streams of high-resolution raw timing data were used to construct a histogram of counts for each pixel. Each time stamp corresponding to a transmitted laser pulse was used as a timing reference point. Between each transmitted laser pulse, the time stamps corresponding to detector events were added to a histogram with total duration equal to the laser pulse repetition period.

Each individual detector event, some of which correspond to photons returned from the target, is an independent measurement of the distance. In an ideal time-of-flight system, only one single-photon returned from the target would be sufficient to make a measurement of the distance to the target. However, uncertainty is introduced into the distance measurement from several factors, including timing jitter (from the master clock, the laser driver, the Si-SPAD and the TCSPC electronics) and spurious counts arising from detector dark noise and a contribution from other light sources, most typically that of the solar background. Hence, it is necessary to utilize multiple counts, corresponding to many transmitted pulses. The effect of timing jitter will be evident as a broadening of the peak in the histogram and the effect of spurious counts is an increase in the overall background counts. A cross-correlation algorithm was used to identify the peak corresponding to the target return by correlating it with a known detector response [21]. By measuring the distance to the target object at each pixel, a depth can be estimated. To reduce the amount of data processing, in cases where the approximate range to the target was known, it was possible to restrict the portion of the histogram that was checked for a correlation to the depth region near the expected range.

Many rangefinders use a low pulse repetition frequency to ensure that only one pulse is in transit at one time [3] to avoid ambiguity in the absolute range by aliasing from adjacent optical pulses. In the measurements presented in this paper, we used frequencies of up to 2 MHz, since depth profiling could be achieved without the concern of range ambiguity—the approximate target depth being unambiguously determined via low repetition frequency measurements. It is possible to increase the pulse repetition frequency provided that the period between successive laser pulses exceeds the return time of flight between the points that define the maximum surface separation within the depth image. Without having *a priori* knowledge of the scene being scanned, the implementation of the system as described here would require that the object of interest is in isolation and has a limited range of depth. In these measurements, the maximum pulse repetition frequency was limited by the first generation of the custom control software but later software versions have since permitted much higher laser repetition rates. Techniques based on the use of a pseudorandom modulated laser output have been used to overcome the problem of range ambiguity in lidar systems, e.g., [22,23]. More recently, a similar approach [24] has been used for the complete avoidance of range ambiguity at high laser frequencies in photon-counting systems, although this technique has not been implemented in the results presented here. The approach described in [24] is fully compatible with the low-power semiconductor laser diode sources used in this work.

5. Experimental Results

The current system presented in this paper was developed as a generic test bed and used many multifunction devices with additional features surplus to those required for a fixed, known application scenario. The system was capable of operation at frequencies in the range of a few kHz up to 2 MHz and measurements were performed using several of these frequencies over a range of different ambient conditions. Table 2 summarizes the key scan parameters for two representative depth profile measurements that were performed with the system, while Figs. 5 and 6 show the depth profiles obtained.

The solar background count rate depended both on weather conditions and on the angle of the Sun relative to the scanning head and was typically in the range of 3000 to 15,000 counts/s when observed in daylight conditions. These solar background measurements were taken with the system pointing in the direction of a reference target to make comparative assessments. The reference target was located at a range of 325 m and was a large sheet of white retroreflective material of a type similar to that used for British car license plates. The transceiver sensor head was situated in a rooftop laboratory and

Table 2. Information on Two Representative Depth Profile Measurements

Object	Image[a]	Conditions	Range (m)	Scan Dimensions (width × height (m))	Resolution of Scanned Image (pixels)	Field of view[b] (mrad)	Pulse Repetition Frequency (kHz)	Approximate Power[c] (μW)	Pixel Dwell Time (s)
Car	Fig. 5	Outdoors at dusk	330	4.0 × 1.2	200 × 64	12	350	10	1.0
Mannequin	Fig. 6	Outdoors on sunny day	325	0.8 × 2.0	32 × 128	6	2000	40	1.0

[a]Figures 5 and 6 show the depth profiles obtained for the measurements described in this table.
[b]The field of view column lists the maximum full angle.
[c]Transmitted powers were measured outside the camera lens after the depth profiles had been obtained.

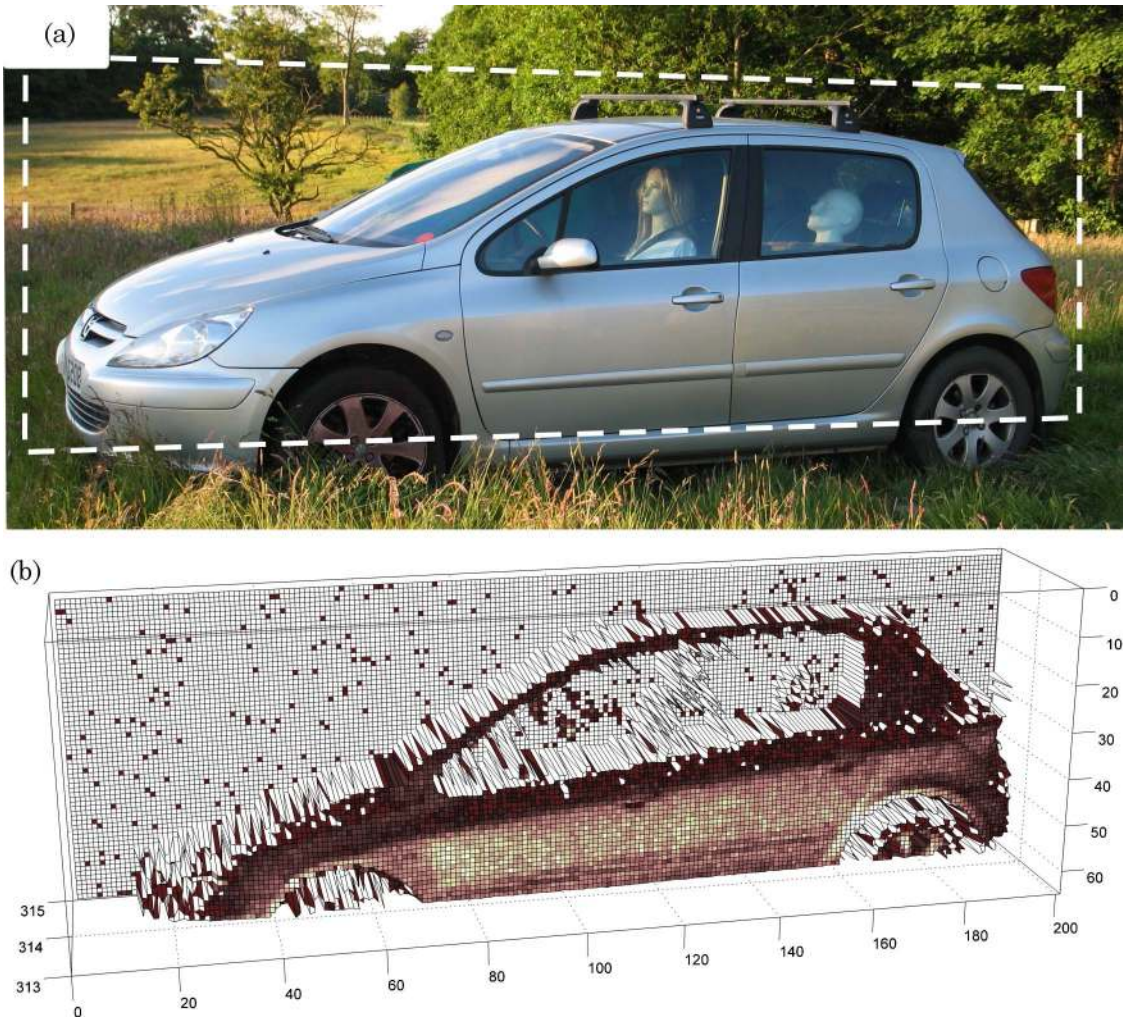

Fig. 5. (Color online) 200 × 64 pixel image of a Peugeot 307 car taken at a distance of 330 m in dusk lighting conditions. (a) Photograph of the car *in situ* on the target range. The dashed box indicates the approximate boundaries of the depth-profile measurement. (b) Depth/intensity image of the car generated from the processed depth information. The colors are defined by the intensity returns from each pixel.

pointed in a southwesterly direction when aligned on the target site. This site was approximately 1° lower in elevation than the rooftop laboratory. As mentioned previously, target distances were limited to ranges of around 325 m due to the available field trial facility and do not represent range limitations of the system, as will be examined in more detail in Section 6.

These results clearly demonstrate photon-counting depth imaging on low-signature targets in a variety of daylight and weather conditions. However, the results were obtained using long overall acquisition times, typically minutes, due to the relatively low laser repetition rates used in this system compared with our previous laboratory-based studies [17]. Also, there was some degree of loss in the system which led to the overall optical energy per pixel used in these measurements being larger than necessary. The required energy per pixel (i.e., $>1\,\mu$J) was similar to that used in depth imaging using linear multiplication detectors [11], albeit our results were at substantially longer range. Both these performance issues are discussed in Section 6 and predictions of possible future performance are given based on these experimental results.

6. Modeling Predictions

The current working system presented in this paper provided a test bed by which the performance of future configurations of the system could be predicted. For example, such analysis provides a means to examine the trade-offs between data acquisition time, optical power, and target range under different operating conditions. The return signal of the target can be characterized in terms of signal-to-noise ratio (SNR). The SNR of a measurement can be defined as in [10]

$$\mathrm{SNR} = \frac{n_p}{\sqrt{n_p + n_b}}, \tag{1}$$

where n_p is the number of counts in the highest channel of the return peak in the time-of-flight histogram

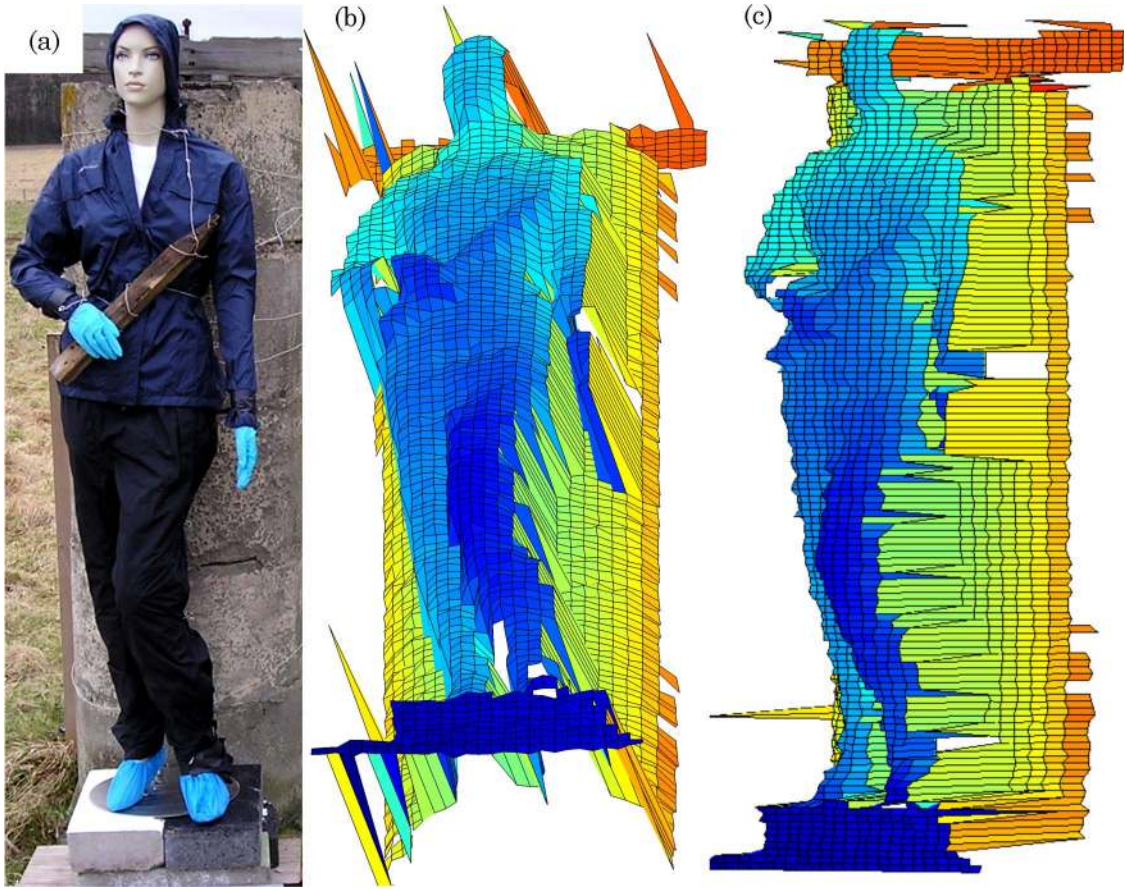

Fig. 6. (Color online) 32 × 128 pixel image of a life-sized mannequin taken at a distance of 325 m in daylight conditions. (a) Photograph of the 1.8 m tall mannequin in the scan position. (b) and (c) Three-dimensional plot of the processed depth information—the curvature of the 600 mm diameter concrete pillar behind the mannequin is clearly evident in (b).

and n_b is the average number of counts per channel in the background. As the background level is reduced, the SNR is dominated by photon statistics of the peak. Such a SNR approach is distinguished from more basic approaches like analysis of the signal-to-background ratio (SBR), which cannot account for the return histogram improving with longer integration times.

The average background level can be estimated for the employed repetition rate f_{Rep} and binning size t_{Bin}, based on averaged total count rates C_{BG} for different environmental conditions with the illuminating laser switched off,

$$n_b = t_{\mathrm{Acq}} C_{\mathrm{BG}} f_{\mathrm{Rep}} t_{\mathrm{Bin}}, \tag{2}$$

where t_{Acq} is the acquisition time per pixel.

The number of illumination photons of wavelength λ leaving the transceiver is readily determined based on the average output power P_{Out} measured in front of the unit. A theoretical model of the system can be created based on this information and taking into account all subsequent photon attenuation stages. The one-way distance r of the scanned object is of relevance both to the atmospheric attenuation encountered during the round trip and due to the divergence of the illumination beam. The extinction coefficient α_{Mod} for the negative exponential relation to distance caused by atmospheric attenuation was simulated for a number of different weather and environmental conditions using the MODTRAN software package [25]. An attenuation factor T_{Mat} is included to consider the significant photon loss due to absorption and reflection of light by the target object that is not aimed back toward the scanning system. T_{Trans} compensates for further attenuation inside the transceiver and caused by the limited detection efficiency of the single-photon detector. T_{Lens} can be used to factor in the effect of changing the system's camera objective. Ultimately, the detector response coefficient (DRC) converts the overall number of returned and detected photons into the number of photons in the maximum bin of the return histogram. Its value is constant for different peak heights but varies when either the binning size or the detector type is changed.

All the factors mentioned are combined to determine n_p:

$$n_P = t_{\mathrm{Acq}} \frac{P_{\mathrm{Out}} \lambda}{\mathrm{hc}} \frac{e^{-\alpha_{\mathrm{Mod}} \times 2r}}{2r^2} \frac{T_{\mathrm{Lens}} T_{\mathrm{Trans}} T_{\mathrm{Mat}}}{\mathrm{DRC}}, \tag{3}$$

where h is Planck's constant and c is the speed of light in vacuum. This allows one to calculate the

achievable SNR in conjunction with Eqs. (1) and (2). Values for the attenuation inherent to the system were determined based on power measurements at different points within the transceiver. Coefficients for different target materials at different incidence angles could be obtained by performing single-pixel scans on a range of materials with all other influencing quantities determined beforehand.

Ultimately, the system is limited by the employed algorithm's ability to reliably detect the instrumental response within a given histogram. In this paper, linear cross-correlation techniques were employed, although other approaches such as maximum likelihood estimation [26] and Markov chain algorithms [27] have previously been used successfully for the detection of low-signature target returns in high background levels in photon-counting time of flight. Such algorithms [27] effectively permit reduced photon return levels to be used for depth imaging, albeit at the expense of increased processing times. Reversible jump Markov chain algorithms allow for the dynamic adaption of the number of degrees of freedom of the system, effectively allowing for analysis of target areas with an unknown number of peak responses [28]. If the procedural method of peak identification within any of these algorithms employs either a mathematical model of the expected system target response or photon return data taken at relatively long integration times as a reference, scintillation effects within analyzed data of shorter acquisition times can cause shape discrepancies detrimental to the algorithm's capability to produce reliable depth estimates. These scintillations predominantly originate from irradiance and return intensity fluctuations due to atmospheric turbulence [29]. A preprocessing step to minimize scintillations in return histograms can be realized with a number of approaches, e.g., implementation of a nonlinear median- or low-pass filter. Additionally, these algorithms can facilitate reliable distance determination in turbid operational environments, such as fog, which can be treated as an intermediate distributed target object, causing a high number of dispersed, low-intensity photon returns.

To determine the minimum SNR value at which the peak finder reliably locks on to a target return for a given binning size, the single-pixel scans mentioned above were analyzed and the returned target range checked for consistency. Once a preliminary minimum SNR value was estimated, additional scans in the suspected regime were performed. The validity of these experiments was verified with additional scans in which the target return was kept constant against a varying background light level, achieved by an external, continuous light source with variable brightness at close range.

An example for the performance of the system in terms of SNR against target range for three target types—aluminum, brass, and foliage—is shown in Fig. 7 under the conditions of a 1 ms acquisition time and a transmit output power of 1 mW. These values

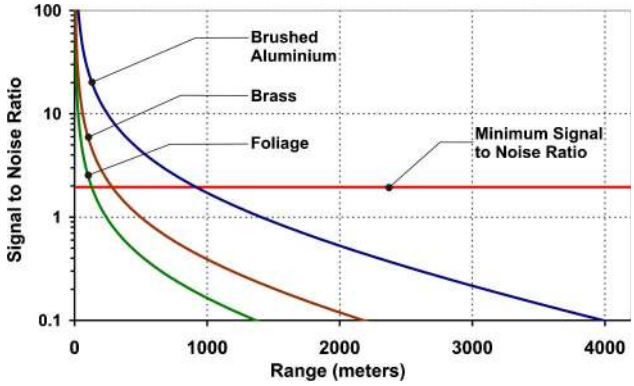

Fig. 7. (Color online) Prediction of SNR versus range for first generation sensor for three different target surfaces at an acquisition time of 1 ms. The model is based on experimental measurements of photon returns. The prediction is for a 40 MHz pulsed laser with average system output power level of 1 mW at 842 nm wavelength. The model assumes overcast daylight conditions. The red line indicates the minimum SNR required for depth measurement using elementary cross-correlation analysis. The model uses MODTRAN estimates for atmospheric transmission in an urban environment.

are chosen to permit the acquisition of a depth image of 32×32 pixels in approximately 1 s, while maintaining eye-safe operation. Also shown in the graph is the minimum SNR detectable using the cross-correlation algorithm. One can see from the graph that, depending on the target material, the sensor will work under these conditions at ranges of less than 1 km.

For longer ranges, the sensor can operate at longer dwell times. However, use of the model does provide the opportunity to examine how system design can affect potential range performance. For example, the sensor design contains three relay lenses that provide a source of backreflections and attenuation in the common transmit and receive channel. These

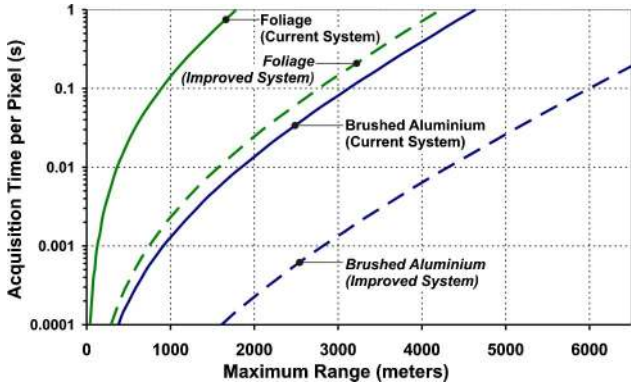

Fig. 8. (Color online) Prediction of maximum detectable range for high- and low-signature targets versus acquisition time, showing predictions for the first generation system and the likely performance of an improved system using a wavelength of 842 nm, a laser repetition frequency of 40 MHz, and an average optical power of 1 mW. Assumptions are based on a reduction of internal system loss by 7 dB, doubling the lens aperture diameter, and adaption of the transmitted spot size. The simulated laser output power, atmospheric conditions, and data analysis method are the same as in Fig. 7.

losses amount to more than 13 dB in the receive channel between the camera lens and the optical fiber connected to the detector. While some of these losses are unavoidable (for example, a 3 dB loss due to filtering of unwanted polarization states at the polarizing beam splitter), there is considerable scope to reduce them in this first generation prototype. A partial redesign of the system could decrease attenuation by an estimated 7 dB. In conjunction with a new camera objective providing a larger diameter collection aperture and infrared-optimized transmission, significantly improved SNR values at identical dwell times will be achievable. Figure 8 shows a summary of these investigations for the two standard target surfaces by comparing the predicted range against acquisition time for the current system and the improved version. These improvements in optical design provide far greater potential for improved range and/or reduced acquisition time for the scanning sensor than optimization of histogram processing.

7. Conclusions

We have demonstrated a scanning time-of-flight depth sensor with an individual photon-timing detector used in conjunction with galvanometer-mirror scanning. The sensor has been used in daylight conditions to construct depth images of noncooperative targets at ranges of 325 m with μW output power levels with centimeter spatial and depth resolution. This low average optical power means that eye-safe power levels can still be maintained despite the predicted increase in laser repetition rate required for more rapid data acquisition, as described in Section 6. Analyses of the trade-off between target range, acquisition time, and optical power have been made and future work on the sensor will concentrate on reducing the losses in the receive channel and investigating a larger diameter collection aperture objective. Theoretical modeling of the system has shown that this approach is capable of the rapid acquisition of depth images at kilometer range. This will require further work to increase the maximum usable laser repetition frequency, which is currently limited by backreflection from the complex optical system. Work is in progress to operate the sensor at a laser frequency of ~100 MHz. The introduction of a nonperiodic pulse pattern to avoid range ambiguity between closely spaced optical pulses, as recently demonstrated by the group [24], means that such high repetition rates will not compromise the range accuracy or even the maximum depth of field possible in a depth image. This current system demonstrates improved depth resolution to other photon-counting outdoor depth imaging systems and comparable, or improved, spatial resolution. Despite optical losses in the system configuration described in this paper, this sensor is capable of operation at lower optical energies per pixel than similar sensors operating using linear multiplication avalanche photodiodes [11], if operated at the same range.

The scanning system is inherently flexible and easily reconfigurable, particularly in terms of the objective lens and the detector. The focal length of the objective lens is a key factor in determining the x – y spatial resolution, and its aperture affects the target return fraction. In terms of single-photon detectors, the single-mode optical fiber delivery means that other detectors can be easily integrated into the system. The measurements shown in this paper indicate that potentially improved performance can be achieved with alternative, low-jitter single-photon detectors such as shallow-junction Si SPADs [30]. Other future studies may utilize the low attenuation and eye-safe, atmospheric transmission window at 1550 nm using new infrared single-photon detectors, such as InGaAs/InP SPAD [13] or NbN superconducting nanowire single-photon detectors [31]. While such single-photon detector technology may be significantly less developed than Si, the use of such a scanning platform means that such detectors can be employed, even when they are necessarily of small active area and used in cooled packages. Further work will also investigate the implementation of data analysis algorithms suitable for analysis of distributed targets, such as partially hidden targets, as used previously in laboratory-based studies [26].

The work reported in this paper was funded by the Electro-Magnetic Remote Sensing (EMRS) Defence Technology Centre, established by the UK Ministry of Defence and run by a consortium of SELEX Sensors and Airborne Systems (now SELEX Galileo), Thales Defence, Roke Manor Research and Filtronic. The authors thank their colleagues and collaborators for their valuable contributions and discussions: Peter Heron, Mark Stewart, Ian Chalmers, Fabian Gutjahr, and Sergio Hernandez-Marin (all Heriot-Watt University), Phil Gorman (QinetiQ), Philip Hiskett and Robert Lamb (both SELEX Galileo, Edinburgh), and Michael Wahl (PicoQuant).

References

1. F. Chen, G. M. Brown, and M. M. Song, "Overview of three-dimensional shape measurement using optical methods," Opt. Eng. **39**, 10–22 (2000).
2. M. C. Amann, T. Bosch, M. Lescure, R. Myllyla, and M. Rioux, "Laser ranging: a critical review of usual techniques for distance measurement," Opt. Eng. **40**, 10–19 (2001).
3. C. Mallet and F. Bretar, "Full-waveform topographic lidar: state-of-the-art," ISPRS J. Photogramm. Remote Sens. **64**, 1–16 (2009).
4. M. A. Albota, R. M. Heinrichs, D. G. Kocher, D. G. Fouche, B. E. Player, M. E. O'Brien, B. F. Aull, J. J. Zayhowski, J. Mooney, B. C. Willard, and R. R. Carlson, "Three-dimensional imaging laser radar with a photon-counting avalanche photodiode array and microchip laser," Appl. Opt. **41**, 7671–7678 (2002).
5. J. J. Degnan, "Photon-counting multikilohertz microlaser altimeters for airborne and spaceborne topographic measurements," J. Geodyn. **34**, 503–549 (2002).
6. C. Ho, K. L. Albright, A. W. Bird, J. Bradley, D. E. Casperson, M. Hindman, W. C. Priedhorsky, W. R. Scarlett, R. C. Smith, J. Theiler, and S. K. Wilson, "Demonstration of literal

three-dimensional imaging," Appl. Opt. **38**, 1833–1840 (1999).
7. R. M. Marino and W. R. Davis, "Jigsaw: a foliage-penetrating 3D imaging laser radar system," Lincoln Lab. J. **15**, 23–36 (2005).
8. J. S. Massa, A. M. Wallace, G. S. Buller, S. J. Fancey, and A. C. Walker, "Laser depth measurement based on time-correlated single-photon counting," Opt. Lett. **22**, 543–545 (1997).
9. W. C. Priedhorsky, R. C. Smith, and C. Ho, "Laser ranging and mapping with a photon-counting detector," Appl. Opt. **35**, 441–452 (1996).
10. S. Pellegrini, G. S. Buller, J. M. Smith, A. M. Wallace, and S. Cova, "Laser-based distance measurement using picosecond resolution time-correlated single-photon counting," Meas. Sci. Technol. **11**, 712–716 (2000).
11. B. W. Schilling, D. N. Barr, G. C. Templeton, L. J. Mizerka, and C. W. Trussell, "Multiple-return laser radar for three-dimensional imaging through obscurations," Appl. Opt. **41**, 2791–2799 (2002).
12. G. S. Buller, R. D. Harkins, A. McCarthy, P. A. Hiskett, G. R. MacKinnon, G. R. Smith, R. Sung, A. M. Wallace, R. A. Lamb, K. D. Ridley, and J. G. Rarity, "Multiple wavelength time-of-flight sensor based on time-correlated single-photon counting," Rev. Sci. Instrum. **76**, 083112 (2005).
13. G. S. Buller, R. E. Warburton, S. Pellegrini, J. S. Ng, J. P. R. David, L. J. J. Tan, A. B. Krysa, and S. Cova, "Single-photon avalanche diode detectors for quantum key distribution," IET Optoelectron. **1**, 249–254 (2007).
14. P. Gatt, S. Johnson, and T. Nichols, "Geiger-mode avalanche photodiode ladar receiver performance characteristics and detection statistics," Appl. Opt. **48**, 3262–3276 (2009).
15. D. G. Fouche, "Detection and false-alarm probabilities for laser radars that use Geiger-mode detectors," Appl. Opt. **42**, 5388–5398 (2003).
16. J. S. Massa, G. S. Buller, A. C. Walker, S. Cova, M. Umasuthan, and A. M. Wallace, "Time-of-flight optical ranging system based on time-correlated single-photon counting," Appl. Opt. **37**, 7298–7304 (1998).
17. J. Massa, G. Buller, A. Walker, G. Smith, S. Cova, M. Umasuthan, and A. Wallace, "Optical design and evaluation of a three-dimensional imaging and ranging system based on time-correlated single-photon counting," Appl. Opt. **41**, 1063–1070 (2002).
18. C. Niclass, A. Rochas, P. A. Besse, and E. Charbon, "Design and characterization of a CMOS 3-D image sensor based on single photon avalanche diodes," IEEE J. Solid-State Circuits **40**, 1847–1854 (2005).
19. D. T. Neilson, S. M. Prince, D. A. Baillie, and F. A. P. Tooley, "Optical design of a 1024-channel free-space sorting demonstrator," Appl. Opt. **36**, 9243–9252 (1997).
20. C. P. Barrett, P. Blair, G. S. Buller, D. T. Neilson, B. Robertson, E. C. Smith, M. R. Taghizadeh, and A. C. Walker, "Components for the implementation of free-space optical crossbars," Appl. Opt. **35**, 6934–6944 (1996).
21. R. E. Warburton, A. McCarthy, A. M. Wallace, S. Hernandez-Marin, R. H. Hadfield, S. W. Nam, and G. S. Buller, "Subcentimeter depth resolution using a single-photon counting time-of-flight laser ranging system at 1550 nm wavelength," Opt. Lett. **32**, 2266–2268 (2007).
22. N. Takeuchi, H. Baba, K. Sakurai, and T. Ueno, "Diode-laser random-modulation cw lidar," Appl. Opt. **25**, 63–67 (1986).
23. N. Takeuchi, N. Sugimoto, H. Baba, and K. Sakurai, "Random modulation cw lidar," Appl. Opt. **22**, 1382–1386 (1983).
24. P. A. Hiskett, C. S. Parry, A. McCarthy, and G. S. Buller, "A photon-counting time-of-flight ranging technique developed for the avoidance of range ambiguity at gigahertz clock rates," Opt. Express **16**, 13685–13698 (2008).
25. A. Berk, L. S. Bernstein, and D. C. Robertson, "MODTRAN: A moderate resolution model for LOWTRAN 7," Technical Note GL-TR-89–0122, available from Geophysics Laboratory/OPE, Air Force Systems Command, Hanscom AFB, Mass., 1989.
26. A. M. Wallace, R. C. W. Sung, G. S. Buller, R. D. Harkins, R. E. Warburton, and R. A. Lamb, "Detecting and characterising returns in a pulsed ladar system," IEE Proc. Vision Image Signal Process. **153**, 160–172 (2006).
27. S. Hernandez-Marin, A. M. Wallace, and G. J. Gibson, "Multilayered 3D LiDAR image construction using spatial models in a Bayesian framework," IEEE Trans. Pattern Anal. Mach. Intell. **30**, 1028–1040 (2008).
28. P. J. Green, "Reversible jump Markov chain Monte Carlo computation and Bayesian model determination," Biometrika **82**, 711–732 (1995).
29. W. P. Cole, M. A. Marciniak, and M. B. Haeri, "Atmospheric-turbulence-effects correction factors for the laser range equation," Opt. Eng. **47**, 126001 (2008).
30. M. Ghioni, A. Gulinatti, I. Rech, F. Zappa, and S. Cova, "Progress in silicon single-photon avalanche diodes," IEEE J. Sel. Top. Quantum Electron. **13**, 852–862 (2007).
31. M. J. Stevens, R. H. Hadfield, R. E. Schwall, S. W. Nam, R. P. Mirin, and J. A. Gupta, "Fast lifetime measurements of infrared emitters using a low-jitter superconducting single-photon detector," Appl. Phys. Lett. **89**, 031109 (2006).